Applied Catalysis B: Environmental 312 (2022) 121410

Contents lists available at ScienceDirect

Applied Catalysis B: Environmental

journal homepage: www.elsevier.com/locate/apcatb

Hydroxylamine enables rapid heterogeneous-homogeneous coupled Fenton sulfamethazine degradation on ferric phosphate

Hanjie Zhang [a], Linghan Li [a], Na Chen [b], Haijie Ben [b], Guangming Zhan [b], Hongwei Sun [b,*], Qin Li [a], Jie Sun [c], Lizhi Zhang [b,*]

[a] School of Chemistry and Materials Science, South-central University for Nationalities, Wuhan 430074, PR China
[b] Key Laboratory of Pesticide & Chemical Biology of Ministry of Education, Institute of Environmental & Applied Chemistry, College of Chemistry, Central China Normal University, Wuhan 430079, PR China
[c] College of Resources and Environmental Science, South-central University for Nationalities, Wuhan 430074, PR China

ARTICLE INFO

Keywords:
Ferric phosphate
Hydroxylamine
Heterogeneous-homogeneous coupled Fenton
Iron cycle
Antibiotic removal

ABSTRACT

Heterogeneous-homogeneous coupled Fenton (HHCF) processes compromise the merits of rapid degradation and catalyst reusability, thus are very attractive for environmental remediation and water treatment. However, the development of HHCF processes suffers from the lack of desirable catalysts and Fe(III)/Fe(II) redox cycle (iron cycle) mediators. Herein we demonstrate the combination of hydrogen peroxide, ferric phosphate and hydroxylamine offers a promising HHCF process, where ferric phosphate and hydroxylamine serve as the catalyst and iron cycle mediator, respectively. Hydroxylamine can realize suitable iron release from ferric phosphate, effective iron cycle, and •OH consumption, resulting in efficient conversion of H_2O_2 to •OH for sulfamethazine removal. More importantly, the phosphorus release from ferric phosphate and nitrogen residual during this HHCF process are limited to reduce the risk of secondary pollution. This study clarifies the importance of iron dissolution and iron cycle on highly efficient Fenton processes, and also provides a promising antibiotic pollutant removal strategy.

1. Introduction

Fenton reaction has been extensively explored as an advanced oxidation process (AOP) to produce highly reactive •OH for pollution control and water treatment [1–4]. The classic homogeneous Fenton reaction is highly efficient in producing •OH, but still faced with several drawbacks including acidic working pH (2−4), massive iron sludge production, and fast attenuation of •OH producing capacity with prolonged time, due to the fast depletion of Fe^{2+} and insufficient reduction of Fe^{3+}, which undergoes hydrolysis and precipitation to generate iron sludge. Moreover, excessive Fe^{2+} significantly scavenges •OH ($k = 3 \times 10^8$ L mol^{-1}s^{-1}) [5]. To overcome these problems, heterogeneous Fenton reactions have been developed, often by using iron-bearing minerals like hematite (α-Fe_2O_3), magnetite (Fe_3O_4), and goethite (α-FeOOH) as catalysts [6–13]. In a typical heterogeneous Fenton reaction, the decomposition of H_2O_2 could be catalyzed by the active ≡Fe sites on the surface of iron minerals, thus avoiding the production of iron sludge, and also extending the working pH range to neutral conditions [14–16]. Nontheless, the oxidation performances of heterogeneous Fenton reactions with iron (hydro)oxides are not satisfactory because of the following reasons: (1) the slow mass transfer processes at the iron (hydro)oxides-solution interface, including the diffusion of H_2O_2 and target pollutants to catalyst surface, the adsorption of reactants, and the desorption of products; (2) the competitive adsorption of H_2O_2 and target pollutants; (3) the scavenge of surface generated •OH by ≡Fe(II) and concentrated H_2O_2 near the surface; (4) the insufficient generation of ≡Fe(II) active sites [14].

It is well known that iron leaching takes place in many heterogeneous Fenton reactions, and the leached iron can remarkably accelerate the overall Fenton oxidation via homogeneous Fenton reactions [14,17,18], because the activation energy of homogeneous Fenton reaction is lower than that of the heterogeneous counterpart [14,19]. We thus believe that it would be beneficial to develop the heterogeneous-homogeneous coupled Fenton (HHCF) processes, in which the heterogeneous catalysts realize the controlled leaching of iron ions to catalyze the homogeneous Fenton reactions, bearing the advantages of high oxidation performance, reusability of heterogeneous catalyst, reduced iron sludge, and less •OH scavenging. Theoretically,

* Corresponding authors.
E-mail addresses: sunhw@ccnu.edu.cn (H. Sun), zhanglz@ccnu.edu.cn (L. Zhang).

https://doi.org/10.1016/j.apcatb.2022.121410
Received 2 February 2022; Received in revised form 27 March 2022; Accepted 12 April 2022
Available online 14 April 2022

highly efficient HHCF processes must satisfy several requirements as follows. First, the rational choice of suitable heterogeneous Fenton catalysts is a prerequisite for the development of HHCF processes. Second, a desirable iron dissolution rate is required to strike a balance between the catalyzed decomposition of H_2O_2, the competitive •OH consumption of Fe^{2+}, and the durability of catalysts. Third, the reduction of Fe^{3+} should be as quick as possible to assure the high rate of •OH production and minimize the precipitation of Fe^{3+}. Unfortunately, the iron dissolution of common iron-bearing minerals during Fenton processes was generally too slow to trigger the coupling of heterogeneous and homogeneous reactions, so chelating agents including succinate, citrate, and ethylene-diaminetetraacetic acid (EDTA) were often adopted to promote the dissolution of iron [20–22], and reductive ligands like ascorbic acid were employed to simultaneously boost the iron dissolution and the reduction of ferric ions [23–30]. Obviously, these chelating agents and reductive ligands are often organic compounds, which might compete •OH with pollutants. Ascorbic acid is a commonly used ligand and reductant to mediate iron cycle of Fenton systems, and thus employed as a reference to check the abilities of different ligands to mediate the redox cycle of Fe(III)/Fe(II) and their side effects of quenching •OH for the development of high-performance HHCF processes in this study.

Different from common iron oxides such as hematite, magnetite, and goethite widely studied as Fenton catalysts, ferric phosphate ($FePO_4$) is an insoluble iron salt with much less attention [31]. As an ionic crystal, $FePO_4$ is supposed to more easily release iron ions than conventional iron oxides, and thus serve as an ideal catalyst to couple heterogeneous and homogeneous Fenton reactions. In this study, we investigated the feasibility of $FePO_4$ for the HHCF removal of a typical antibiotics sulfamethazine (SM2), in comparison with commonly used iron oxides including magnetite (Fe_3O_4) and hematite (Fe_2O_3). Meanwhile, two naturally-occurring small molecular ligands including ascorbic acid (AA) and hydroxylamine (HA) were utilized to promote the iron dissolution and the iron redox cycle for the efficient conversion of H_2O_2 to •OH and the oxidative degradation of SM2, aiming to develop a high-performance HHCF system.

2. Experimental section

2.1. Chemicals

Ascorbic acid (AA), hydrogen peroxide (H_2O_2, 30%), magnetite (Fe_3O_4), hematite (α-Fe_2O_3), ferrous sulfate heptahydrate ($FeSO_4$•$7H_2O$), sodium acetate (CH_3COONa), 1,10-phenanthroline, benzoic acid (BA), *p*-hydroxybenzoic acid (*p*-HBA), sulfuric acid (H_2SO_4), sodium hydroxide (NaOH), sodium fluoride (NaF), potassium dihydrogen phosphate (KH_2PO_4), ammonium molybdate tetrahydrate ($(NH_4)_6Mo_7O_{24}$•$4H_2O$), potassium iodide (KI), ethanol were of analytical grade and purchased from Sinopharm Chemical Reagent Co., Ltd. China. Hydroxylamine hydrochloride (HA), ferric phosphate ($FePO_4$), potassium antimony tartrate ($C_4H_4KO_7Sb$•$0.5H_2O$), potassium hydrogen phthalate were purchased from Aladdin Chemistry Co., Ltd. China. Sulfadimidine (SM2) was purchased from TCI (Shanghai) Development Co., Ltd. Acetonitrile, acetone and methanol were of HPLC grade ($\geq$ 99.9%) and purchased from Merck KGaA.

2.2. Heterogeneous-homogeneous coupled Fenton degradation of SM2

The typical heterogeneous-homogeneous coupled Fenton degradation of SM2 was conducted as follows. 1 mL of SM2 stock solution (250 mg/L) was added to 48 mL of distilled water in a 100 mL conical flask, followed by the addition of 0.02 g of iron-bearing minerals ($FePO_4$, Fe_3O_4 or Fe_2O_3), 0.5 mL of 100 mmol/L AA or HA, and 0.5 mL of 100 mmol/L H_2O_2 to triger the Fenton reaction. The flask was shaken continuously on an orbital shaker to promote the dispersion of iron minerals in the SM2 aqueous solution. Samples were withdrawn at regular time intervals and scavenged by 10% (v/v) absolute ethanol, filtered through 0.22 μm syringe membrane for the determination of SM2 concentrations. Experiments were conducted in the dark to avoid the possible interference of ambient light, and the pH values of the reaction solution were adjusted with diluted H_2SO_4 or NaOH when necessary.

2.3. Analytical methods

The concentrations of SM2 were monitored by high performance liquid chromatography (HPLC, Ultimate 3000, Thermo) equipped with an Agilent SB-C18 column (150 mm × 4.6 mm, 5 μm) and a diode array detector. The mobile phase was composed of 30% acetonitrile and 70% water containing 0.2% acetic acid at the constant flow rate of 1 mL/min. The wavelength of detector was 275 nm [32,33]. Concentrations of AA were monitored by a UV–visible spectrometer within the wavelength of 200–400 nm. Concentrations of H_2O_2 were determined with the iodide colorimetric method following the reported procedures [23]. First, we checked the influence of HA on the measurement of H_2O_2. As expected, the addition of 1 mmol/L HA obviously weakened the UV–vis signal of H_2O_2 centered at 352 nm (Fig. S1a). Since the concentration of HA changed gradually during the $FePO_4$/HA HHCF process, its interference on H_2O_2 quantification would also vary along reaction time, so it was necessary to quench the HA for the accurate quantification of H_2O_2 concentrations. Fortunately, we found that 10% acetone (v/v) was sufficient to scavenge the HA residual and perfectly recover the UV–vis signal of H_2O_2 (Fig. S1a). The calibration curve of H_2O_2 concentrations in the presence of 1 mmol/L HA and 10% acetone were well established (Fig. S1b). HA concentrations were measured as follows [34]. Briefly, 0.9 mL of the sample was taken at regular times and immediately mixed with 0.1 mL of acetone to produce the acetone oxime, which was quantified with HPLC. The accumulative amount of •OH were probed with BA oxidation, with the •OH adduct *p*-HBA detected by the HPLC method, and the accumulative •OH concentration is 5.87 times that of *p*-HBA [35,36]. The concentrations of dissolved iron ions were determined by a modified 1,10-phenanthroline chromogenic method [37]. Briefly, samples were filtered through 0.22 μm syringe membranes, then 0.5 mL filtrate were immediately mixed with 0.5 mL distilled water, 1 mL 2 g/L 1,10-phenanthroline, and 1 mL 10% CH_3COONa, and the absorbance at 510 nm was measured to determine the concentrations of Fe^{2+} with the calibration curve. For the analysis of total dissolved iron ions, 0.5 mL of sample was first added with 0.5 mL 100 g/L HA, followed by the addition of 1 mL 2 g/L 1,10-phenanthroline and 1 mL 10% CH_3COONa for absorbance measurement. The concentrations of total dissolved phosphorus in the bulk solution after the heterogeneous-homogeneous coupled Fenton reaction with $FePO_4$ were quantified with the ammonium molybdate spectrophotometric method (GB 11893-89, China). The concentrations of NH_4^+, NO_2^- and NO_3^- were measured with ionic chromatography (DIONEX ICS-900, Thermo Scientific, U.S.A.), and concentrations of the total dissolved nitrogen (TN) were analyzed following the standard procedure of the alkaline potassium persulfate digestion-UV spectro photo metric method (GB 11894-89, China). The degrading intermediates of SM2 were verified using liquid chromatography-mass spectrometry equipped with tandem mass spectrometry (HPLC-MS/MS, Ultimate 3000 UHPLC-Q Exactive, Thermo Scientific, U.S.A.), in the positive mode with a HESI ion source. The full scans within *m/z* of 50–500 were adopted to collect the primary mass spectra, and the dependent scan events were conducted to obtain the spectra of secondary ions after collision. A nitrogen-adsorption system (Micrometritics ASAP2010) was employed to record the adsorption-desorption isotherms of iron bearing minerals at the liquid-nitrogen temperature of 77 K. The total organic carbon (TOC) concentrations were measured with a TOC analyzer (TOC-VCPH, Shimadzu, Japan) following the manufacturer's protocol. 5 g/L $Na_2S_2O_3$ was added to quench the Fenton reaction at sampling before TOC tests, and its contribution (ca. 0.48 mg/L TOC) was not subtracted from the

TOC of samples.

3. Results and discussion

3.1. Screening of high-performance HHCF processes

We first characterized $FePO_4$, Fe_3O_4 and Fe_2O_3 by using X-ray diffraction (XRD), scanning electron microscope (SEM) and N_2 adsorption experiments. XRD patterns of three iron bearing minerals matched well with the standard diffraction patterns of $FePO_4$ (PDF #50-1635), Fe_3O_4 (PDF #99-0073) and Fe_2O_3 (PDF #79-1741), respectively, indicating their crystalline nature and phase purity (Fig. S2). SEM images revealed that $FePO_4$ consisted of large aggregates of layered structure with the lamellar thickness of ca. 50 nm (Fig. S3a and S3b). In contrast, Fe_3O_4 was in the shape of octahedral crystals, with size in the range from tens of nanometers to several micrometers (Fig. S3c and S3d), while Fe_2O_3 was composed of irregular spheres or rods with size of tens to hundreds of nanometers (Fig. S3e and S3f). Nitrogen adsorption analysis displayed that the Brunmaner-Emmett-Teller (BET) specific surface areas of $FePO_4$, Fe_3O_4 and Fe_2O_3 were 96, 42, and 65 m^2/g, respectively.

We then checked the performance of $FePO_4$, Fe_3O_4 and Fe_2O_3 on Fenton degradation of SM2, and found that all these three iron-bearing minerals exhibited very poor heterogeneous Fenton activities, which were less than 5% of SM2 degradation within 180 min, because of their negligible iron dissolution and poor iron redox cycling (Fig. 1a). These phenomena were consistent with previous results [23,38]. Regarding that AA could promote magnetite Fenton degradation of alachlor [23], we thus compared the Fenton SM2 degradation performance of $FePO_4$, Fe_3O_4 and Fe_2O_3 in the presence of AA to screen a highly efficient HHCF catalyst. Impressively, the addition of AA significantly increased their Fenton degradation ratios of SM2, which respectively reached 81.7%, 72.0% and 53.4% in 60 min for $FePO_4$, Fe_3O_4 and Fe_2O_3 (Fig. 1b), suggesting that $FePO_4$ might be the most promising HHCF catalyst among the three iron-bearing minerals. The kinetics of SM2 removal across 60 min during the $FePO_4$/AA HHCF process were investigated, but poor fitting results were obtained for both pseudo-first order and pseudo-second order kinetics models, with R^2 of 0.6467 and 0.7758, respectively. Nonetheless, good fitting results were acquired if the SM2 degradation curve was divided into two sections (0–20 min and 20–60 min). Regarding the similar fitting results (R^2) of the two kinetics models, pseudo-first order kinetics was selected for simplicity, and the rate constant fell drastically from 0.0779 min^{-1} (0–20 min) to 0.00522 min^{-1} (20–60 min, Fig. 1c). This degradation rate decrease resulted in the incomplete removal of SM2, which might be arisen from the depletion of AA during the reaction [23].

Different from AA, HA is a common reductive chemical without any organic groups, and also used as the iron cycle mediator for the coupling of heterogeneous and homogeneous Fenton reactions [39–42]. The initial pH of the $FePO_4$/HA HHCF system was ca. 4.3, slightly higher than that (ca. 4.0) of the $FePO_4$/AA HHCF system. For better comparison, the initial pH values of both HHCF reactions were adjusted to 4 with diluted H_2SO_4 solution. Interestingly, the addition of HA sharply accelerated the Fenton oxidation, and 100% of SM2 was removed by the $FePO_4$/HA HHCF process within 120 min (Fig. 2a). Although the pseudo-first order SM2 degradation rate constant (0.0580 min^{-1}) of $FePO_4$/HA HHCF was slightly slower than that (0.0857 min^{-1}) of $FePO_4$/AA HHCF within 20 min, the degradation rate decrease phenomenon did not appear during the whole reaction period of the $FePO_4$/HA HHCF process (Fig. 2b), indicating that HA might be a more efficient HHCF mediator than AA.

We further checked the performance of $FePO_4$, Fe_3O_4 and Fe_2O_3 as the HHCF catalysts in the presence of HA, and compared the SM2 removal efficiencies of three $FePO_4$/HA, Fe_3O_4/HA, and Fe_2O_3/HA HHCF processes (Fig. 2c), whose pseudo-first order rate constants were respectively 1.01×10^{-1}, 2.16×10^{-2}, and 3.15×10^{-3} min^{-1} (Fig. 2d). To rule out the influence of different surface areas of three iron minerals on the performances of different HHCF processes, we normalized the SM2 degradation rate constants of three HHCF processes by three catalysts' specific surface areas, and interestingly found that the normalized rate constant (1.05×10^{-3} g m^{-2} min^{-1}) of $FePO_4$/HA HHCF was ca. 2 times that of Fe_3O_4/HA HHCF (5.15×10^{-4} g m^{-2} min^{-1}), and ca. 22 times that of Fe_2O_3/HA HHCF (4.83×10^{-5} g m^{-2} min^{-1}). These results confirmed that $FePO_4$ was a superior HHCF catalyst to Fe_3O_4 and Fe_2O_3.

More control experiments were then carried out to understand the $FePO_4$/HA HHCF process. As expected, neither H_2O_2 nor $FePO_4$ alone could induce the significant removal of SM2, whereas only 10.8% of SM2 was removed by the HA/H_2O_2 process after 100 min of reaction (Fig. S4a), because HA could react with oxidants like H_2O_2 to produce •OH [29,43,44]. The pseudo-first order SM2 degradation rate constant of $FePO_4$/HA HHCF (0.101 min^{-1}) was 84 times that (1.2×10^{-3} min^{-1}) of HA/H_2O_2 (Fig. S4b). Therefore, the combination of H_2O_2, ferric phosphate and hydroxylamine delivered a highly efficient HHCF process.

3.2. Iron dissolution and iron cycle meditor consumption during different Fenton processes

To further understand the heterogenous-homogeneous Fenton coupling process of $FePO_4$/HA, we first monitored the pH changes during the different Fenton processes. The pH values remained constant at 4 during the $FePO_4$/H_2O_2 and $FePO_4$/AA HHCF processes, but decreased gradually from 4 to 3 during the $FePO_4$/HA HHCF process (Fig. S5), because the oxidation of HA would release proton [29,34]. To check the possible contribution of the lower pH to the enhanced SM2 degradation during the $FePO_4$/HA HHCF process, we compared the SM2

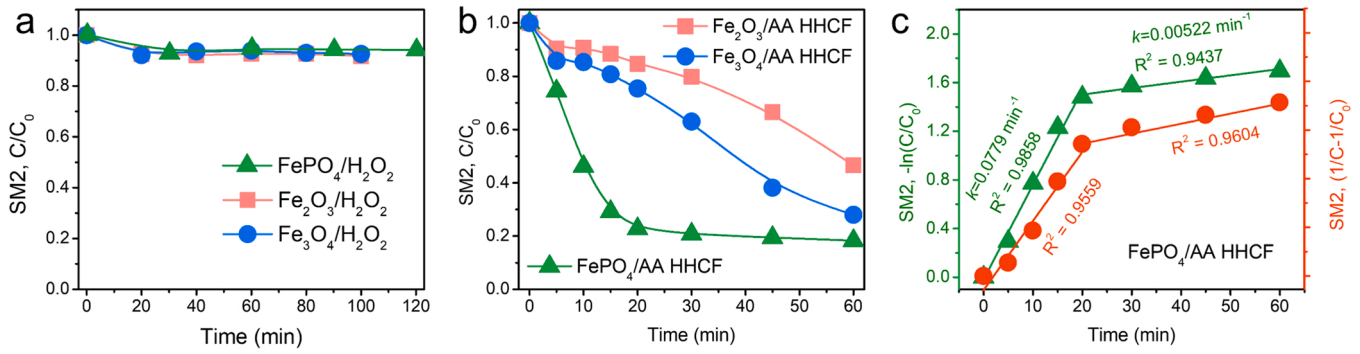

Fig. 1. (a) The removal profiles of SM2 by Fenton processes catalyzed by $FePO_4$ and iron oxides. (b) The SM2 removal profiles of Fenton processes in the presence of AA. (c) The pseudo-first-order (green) and pseudo-second-order (red) kinetics of SM2 removal in the $FePO_4$/AA HHCF process. Conditions: $[SM2]_0 = 5$ mg/L, $[FePO_4]_0 = [Fe_3O_4]_0 = [Fe_2O_3]_0 = 0.4$ g/L, $[H_2O_2]_0 = 5$ mmol/L, $[AA]_0 = 1$ mmol/L. The initial pH values were not adjusted, and those in (b) were ca. 4.0.

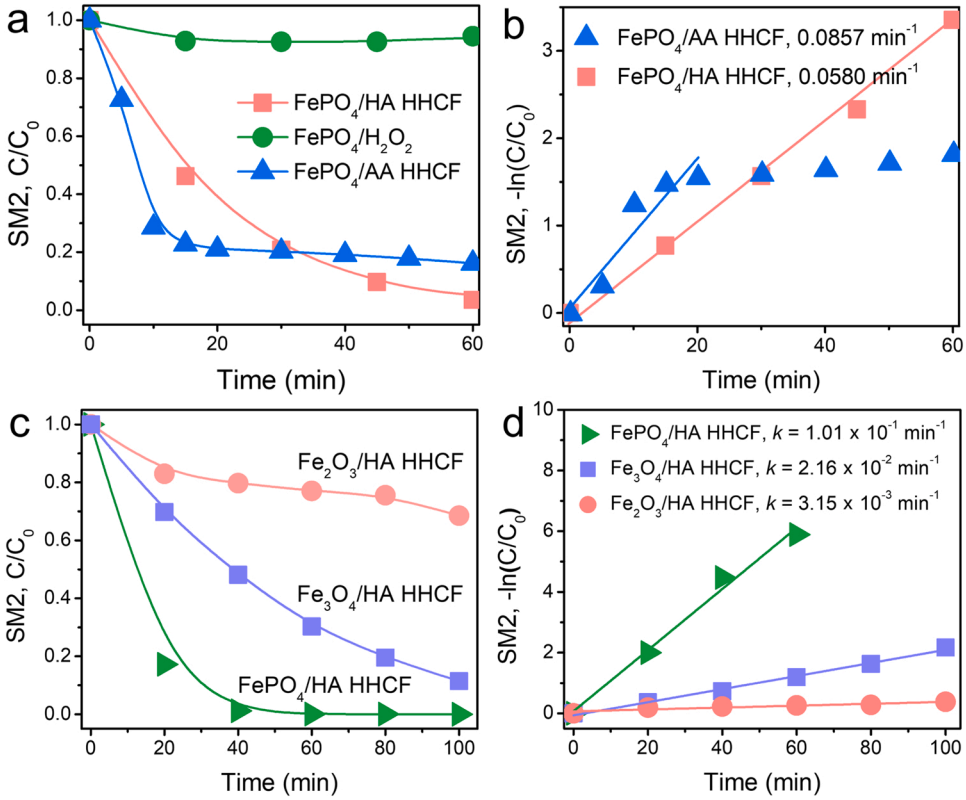

Fig. 2. (a) The comparison of SM2 removal by $FePO_4$/AA and $FePO_4$/HA HHCF processes. (b) The pseudo-first order kinetics curves of SM2 removal by $FePO_4$/AA and $FePO_4$/HA HHCF processes. (c) The comparison of SM2 removal profiles in HA mediated HHCF processes with different iron bearing minerals and (d) the corresponding pseudo-first order kinetics curves. Conditions: $[SM2]_0$ = 5 mg/L, $[FePO_4]_0$ = $[Fe_3O_4]_0$ = $[Fe_2O_3]_0$ = 0.4 g/L, $[H_2O_2]_0$ = 5 mmol/L, $[HA]_0$ = $[AA]_0$ = 1 mmol/L. The initial pH values in (a) and (b) were 4.0, but were not adjusted in (c) and (d), ca. 4.3.

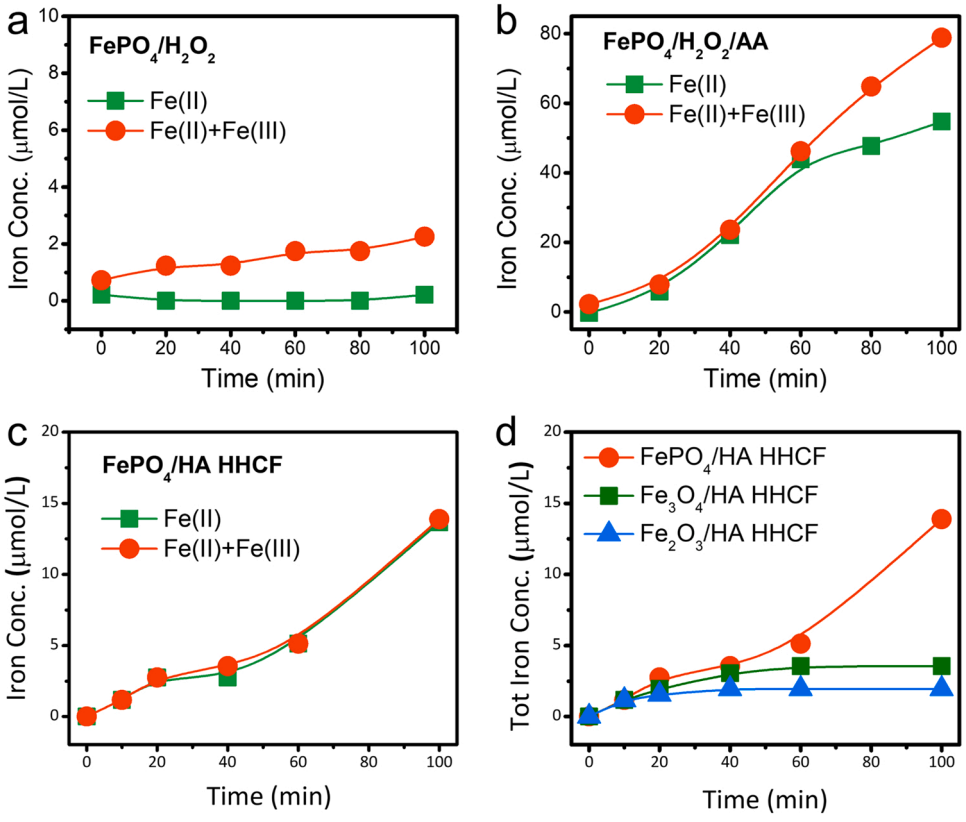

Fig. 3. The profiles of iron dissolution in the (a) $FePO_4/H_2O_2$, (b) $FePO_4$/AA HHCF, and (c) $FePO_4$/HA HHCF processes. (d) The comparison of total dissolved iron concentrations in HA HHCF systems catalyzed by different iron-bearing minerals. Conditions: $[FePO_4]_0$ = $[Fe_3O_4]_0$ = $[Fe_2O_3]_0$ = 0.4 g/L, $[H_2O_2]_0$ = 5 mmol/L, $[AA]_0$ = $[HA]_0$ = 1 mmol/L, initial pH was not adjusted.

degradation efficiencies at the initial pH of 3 and 4, and found that this pH decrease did not change the SM2 degradation performances of $FePO_4/H_2O_2$, but inhibited the SM2 removal by $FePO_4$/AA HHCF process (Fig. S6). These experimental results ruled out the contribution of lower pH to the better performance of $FePO_4$/HA HHCF system.

We then investigated the iron dissolution during the different HHCF processes for comparison. As expected, AA could accelerate both the iron dissolution and the iron redox cycle of $FePO_4$ (Fig. 3a and b), because the concentrations of total dissolved iron and Fe^{2+} increased to 78.8 and 54.7 μmol/L after 100 min of reaction in the presence of AA, much higher than those (2.3 μmol/L of total dissolved iron and 0.2 μmol/L of Fe^{2+} after 100 min) in the absence of AA. The promoted iron dissolution and iron cycle could well explain the improved Fenton removal of SM2 in the presence of AA. As for the $FePO_4$/HA HHCF process, the concentrations of released total iron and Fe^{2+} were 13.9 and 13.7 μmol/L after 100 min, respectively (Fig. 3c). Although HA was less effective than AA on the iron dissolution from $FePO_4$, it was a better iron redox mediator, because the ratio of Fe^{2+} to total iron in case of HA reached 99%, much higher than that of AA (69%). Meanwhile, the dissolution of $FePO_4$ was the most effective in the presence of HA among the three iron bearing minerals. For instance, the total iron concentrations were merely 3.6 μmol/L and 2.0 μmol/L after 100 min for the Fe_3O_4/HA and Fe_2O_3/HA HHCF processes (Fig. 3d), respectively. Therefore, the $FePO_4$/HA HHCF system possessed desirable iron dissolution to strike a balance between the excellent heterogeneous-homogeneous coupled Fenton performance and the durability of the heterogeneous catalyst.

Regarding the indispensable roles of AA and HA in promoting both iron dissolution and iron redox cycle for efficient HHCF reactions, their depletion would significantly influence the SM2 removal during the $FePO_4$ based HHCF processes. During the HHCF processes, AA or HA may be consumed either through the reduction of ferric species either on the surface of $FePO_4$ or in the bulk solution to accelerate the iron redox cycle, or by the oxidative attack from Fenton oxidants like •OH. Obviously, the competitive •OH consumption of AA or HA in the latter case was undesired. Thus, we monitored the time profile of AA concentrations during the $FePO_4$/AA HHCF reaction after ruling out the interference of co-existing species (Fig. S7). The tiny consumption of AA in the control experiments of $FePO_4$/AA and H_2O_2/AA reactions suggested the slow reductive dissolution of $FePO_4$ by AA (Fig. S8a) and the ineffective direct reaction between H_2O_2 and AA (Fig. S8b), respectively. In contrast, AA underwent a fast depletion during the SM2 degradation with $FePO_4$/AA HHCF process, and was nearly exhausted after 20 min (Fig. S8c and Fig. 4a), coincided well with the time profile of SM2 removal (Fig. 1b). Therefore, we believe the fast consumption of AA was responsible for the significantly decreased SM2 removal rate after 20 min in the $FePO_4$/AA HHCF system. This fast depletion of AA might be ascribed to the higher kinetics rate constant between AA and •OH ($k_{AA\text{-}OH} = 1.0 \times 10^{10}$ L mol^{-1} s^{-1}) [23] than that of SM2 and •OH ($7.8 \pm 0.5) \times 10^9$ L mol^{-1} s^{-1}) [45], and the higher initial molar concentration of AA (1 mmol/L) than that of SM2 (0.0180 mmol/L). These two factors resulted in that the initial rate of AA oxidation by •OH was 71.2 times that of SM2 oxidation by •OH. This was further supported by the fact that the presence of SM2 did not significantly affect the consumption of AA during the $FePO_4$/AA HHCF process (Fig. S8d and Fig. 4 a).

Similar with the fate of AA in the $FePO_4$/AA HHCF process, HA might also undergo oxidation by Fe^{3+} or •OH (Eqs. 1–4). Although the control experiments of HA/H_2O_2 and $FePO_4$/HA revealed that the direct reaction between HA and H_2O_2 or $FePO_4$ was negligible (Figs. 4b), 32.1% of HA was consumed after 100 min of reaction during the degradation of SM2 with $FePO_4$/HA HHCF process, which was still much slower than the case of AA. This phenomenon was reasonable because the second rate constant between HA and •OH was just 1.15×10^8 L mol^{-1} s^{-1}, almost 2 orders of magnitude lower than that between AA and •OH. Furthermore, the initial oxidation rate of HA by •OH was only 0.8 times that of SM2 in the $FePO_4$/HA HHCF process, far much lower than that (71.2 times) in the $FePO_4$/AA HHCF. Impressively, 63.4% of HA was consumed after 100 min in the $FePO_4$/HA HHCF process without adding SM2, much faster than that in the presence of SM2. This difference further confirmed that the competitive •OH comsumption of HA was inhibited by the presence of SM2. Therefore, the efficient heterogeneous-homogeneous coupled Fenton SM2 degradation of $FePO_4$/HA HHCF also relied on less competitive •OH comsumption of iron cycle meditor.

$$Fe(III) + NH_3OH^+ = Fe(NH_2OH)^{3+} + H^+ \quad (1)$$

$$Fe(NH_2OH)^{3+} = NH_2O\bullet + H^+ + Fe^{2+} \quad (2)$$

$$\bullet OH + NH_3OH^+ = NH_2O\bullet + H^+ + H_2O \quad (3)$$

$$2NH_2O\bullet = N_2 + H_2O \quad (4)$$

3.3. The conversion of H_2O_2 to •OH during different Fenton processes

We subsequently carefully examined the conversion of H_2O_2 in the $FePO_4$/HA HHCF system. As expected, H_2O_2 was not effectively decomposed within 100 min of reaction in either HA/H_2O_2 or $FePO_4$/H_2O_2 systems, consistent with their poor SM2 removal performances. In contrast, the introduction of HA obviously promoted the conversion of H_2O_2, and 20.3% of H_2O_2 (1.01 mmol/L) was decomposed after 100 min in the $FePO_4$/HA HHCF process (Fig. 5a). Scavenging experiment using tert-butyl alcohol (TBA) demonstrated that •OH was the dominant reactive species responsible for SM2 removal in the $FePO_4$/HA HHCF process (Fig. S9). The production of •OH was subsequently quantified by using benzoic acid as the trapping probe. Continuous

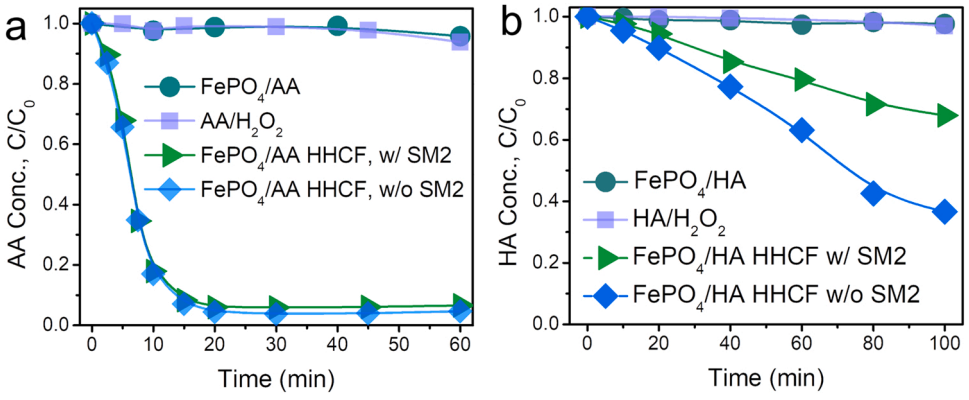

Fig. 4. (a) The concentrations of AA during the $FePO_4$/AA HHCF process and its counterparts. (b) The depletion of HA in the $FePO_4$/HA HHCF and other control processes. Conditions: $[SM2]_0 = 5$ mg/L, $[FePO_4]_0 = 0.4$ g/L, $[H_2O_2]_0 = 5$ mmol/L, $[AA]_0 = [HA]_0 = 1$ mmol/L, initial pH was not adjusted.

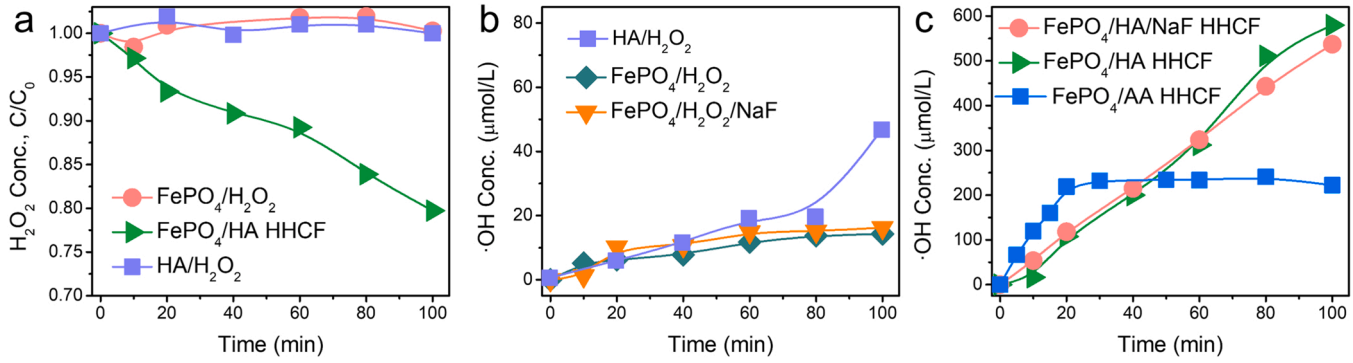

Fig. 5. (a) The decomposition profiles of H_2O_2 in $FePO_4$/HA HHCF reactions. (b) The accumulation of •OH concentration in $FePO_4/H_2O_2$ and HA/H_2O_2 control processes. (c) The accumulated •OH in the $FePO_4$/HA and $FePO_4$/AA HHCF reactions. Conditions: $[SM2]_0 = 5$ mg/L, $[FePO_4]_0 = 0.4$ g/L, $[H_2O_2]_0 = 5$ mmol/L, $[HA]_0 = 1$ mmol/L, $[NaF]_0 = 0.05$ mmol/L, initial pH was not adjusted.

accumulation of •OH was observed in the control experiments of $FePO_4/H_2O_2$ and HA/H_2O_2 reactions, with 14.3 and 46.6 μmol/L •OH accumulated after 100 min, respectively (Fig. 5b). Impressively, much more accumulative •OH (579.4 μmol/L) was produced in the $FePO_4$/HA HHCF process (Fig. 5c). Regarding that surface-associated •OH could be generated during some heterogeneous Fenton-like reactions [46], we also measured the concentrations of •OH with the addition of 0.05 mmol/L NaF, which could liberate the surface-confined •OH by ligand exchange effect [28]. However, the addition of NaF did not increase the •OH concentrations in either the $FePO_4/H_2O_2$ or $FePO_4$/HA HHCF processes (Fig. 5b and c), indicating that most of •OH was in the bulk solution rather than surface-confined in this study. The conversion efficiency of H_2O_2 to •OH ([•OH] produced/[H_2O_2] consumed) was 57.4% in the $FePO_4$/HA HHCF process, according to the stoichiometry of •OH production in the Fenton process (Eq. 5). On the contrary, the production of •OH during the $FePO_4$/AA HHCF process was very fast in the initial 20 min, but leveled off thereafter, with 222.1 μmol/L •OH accumulated in 100 min, much less than that (579.4 μmol/L) in the $FePO_4$/HA HHCF process (Fig. 5c). These results suggested that HA could greatly promote the conversion of H_2O_2 to •OH on $FePO_4$.

$$Fe(II) + H_2O_2 \rightarrow Fe(III) + \bullet OH + OH^- \quad (5)$$

For comparison, we also investigated the decomposition of H_2O_2, the production of •OH, and the consumption of HA in the Fe_3O_4/AA HHCF and Fe_2O_3/HA HHCF processes. Similar with the case of $FePO_4/H_2O_2$, the production of •OH was also negligible in the Fe_3O_4/H_2O_2 (5.3 μmol/L) and Fe_2O_3/H_2O_2 (7.6 μmol/L) processes within 100 min (Fig. S10a and S10b). The accumulated •OH after 100 min in the Fe_3O_4/AA HHCF and Fe_2O_3/HA HHCF processes respectively increased to 212.6 and 140.1 μmol/L, much less than that (579.4 μmol/L) of $FePO_4$/HA HHCF. Accordingly, the decomposition percentages of H_2O_2 were respectively 4.7% and 1.2% within 100 min for the Fe_3O_4/AA HHCF and Fe_2O_3/HA HHCF processes (Fig. S10c and S10d), also much lower than that (20.3%) of $FePO_4$/HA HHCF process, confirming that the combination of H_2O_2, ferric phosphate and hydroxylamine could produce a highly efficient HHCF process. As expected, the consumptions of HA in the Fe_3O_4/HA, Fe_3O_4/HA HHCF, Fe_2O_3/HA and Fe_2O_3/HA HHCF were also much less than that in the $FePO_4$/HA HHCF process (Fig. S10e and S10f).

3.4. The reusability of $FePO_4$ and the safety of $FePO_4$/HA HHCF process

The application of $FePO_4$ as the catalyst of HHCF processes might bring the secondary phosphorous pollution problem owing to its phosphorous release. To check this issue, we tracked the release of phosphorus within a relatively long reaction period of 300 min. Continuous release of phosphorus was observed in the $FePO_4$/HA HHCF reaction, because HA induced reductive dissolution of Fe from $FePO_4$ would accompany with the release of adjacent phosphate groups. Fortunately, the concentration of dissolved phosphorus was low across the reaction period, with total 0.65 mg/L P released after 300 min (Fig. 6a), still below the guideline (1 mg/L) regulated by the Integrated Wastewater Discharge Standard of China (GB 8978–1996) and the Discharge Standard of Pollutants for Municipal Wastewater Treatment Plant (GB 18918-2002, China). In real water treatment scenarios, the hydraulic retention time can be optimized to further minimize the dissolution of phosphorus. The durability of $FePO_4$ was further investigated by collecting the catalyst after 60 min of reaction for reuse. Even at the fourth cycle of reaction, the used $FePO_4$ still exhibited similar SM2 removal efficiency and morphology with the pristine one (Fig. 6b and c), further confirming that $FePO_4$ was a superior HHCF catalyst of excellent reusability. The impact of coexisted ions in natural and wastewater were also investigated. As shown by Fig. S11, the presence of bicarbonate slightly inhibited the removal of SM2 depending on the concentration of bicarbonate, but SM2 can still be removed continuously even in the presence of 10 mmol/L bicarbonate. Impressively, sulfate and chloride significantly promote the removal of SM2. These results suggest that the $FePO_4$/HA HHCF process is robust against the influence of coexisted ions.

To elucidate the fate of SM2 during the $FePO_4$/HA HHCF process, we further employed the HPLC-MS/MS technique to identify the degradation intermediates of SM2 by analyzing the *m/z* values of various fragments [47–50]. Besides the parent substrate SM2, seven degradation intermediates were detected (Figs. S12-S19). We also monitored the TOC concentrations of the SM2 solution during the $FePO_4$/HA HHCF process, and the TOC decreased by ca. 18.2% across 180 min of reaction, much slower than the degradation of SM2 (Fig. S20). Based on these intermediates and TOC profiles, we proposed the possible degrading pathways of SM2 during the $FePO_4$/HA HHCF process (Scheme 1). First, •OH attacked the aniline group of SM2 to generate various intermediates, including the OH-adduct, 4-amino-N-(4,6-dimethylpyrimidin-2-yl)-3,5-dihydroxybenzenesulfonamide (P310), and the deamination product, N-(4,6-dimethylpyrimidin-2-yl)benzenesulfonamide (P263). Meanwhile, •OH also induced the cleavage of the sulfanilamide bond to produce 4-aminobenzenesulfonic acid (P173) and 4,6-dimethylpyrimidin-2-amine (P123). P173 might undergo a de-sulfonyl process with the OH addition to generate 4-aminophenol (P109). Whereas P123 might be oxidized by •OH either to 2-amino-4,6-dimethylpyrimidin-5-ol (P139) through the OH addition, or to 2-amino-6-methylpyrimidine-4-carboxylic acid (P153) via the oxidation of methyl group. These intermediates might be further degraded, and even mineralized to inorganic species including CO_2, H_2O, NH_4^+ or NO_x. The detailed transformation of nitrogen in both HA and SM2 were also investigated by measuring the concentrations of nitrogen-containing species including HA, SM2, NH_4^+, NO_2^-, NO_3^-, and dissolved total nitrogen (TN). For the $FePO_4$/HA HHCF system without adding SM2, the initial TN was 12.8 mg/L, close to the theoretical N concentration of

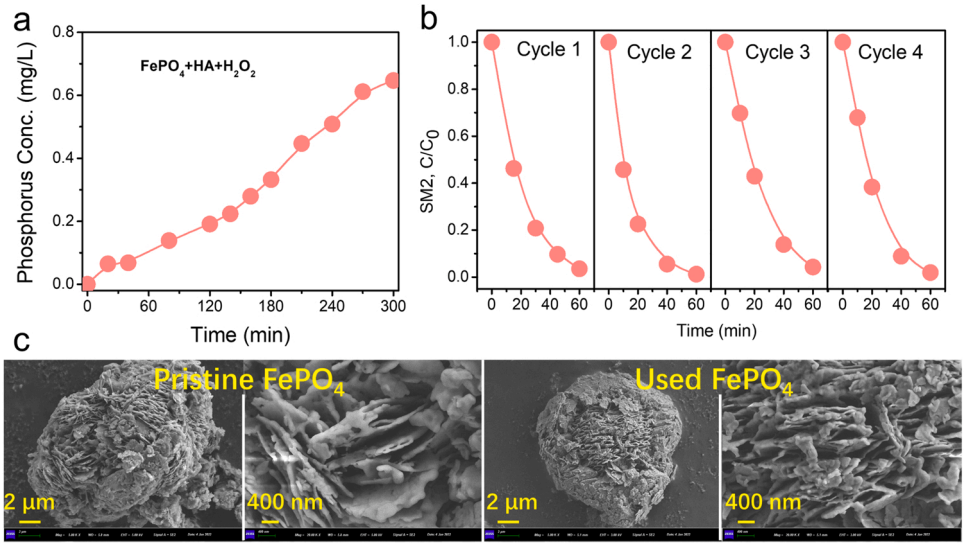

Fig. 6. (a) The concentrations of phosphorus released into the bulk solution during the $FePO_4$/HA HHCF reaction. (b) The reusability of $FePO_4$ as the catalyst in the $FePO_4$/HA HHCF reactions. (c) The SEM images of pristine $FePO_4$ and that collected after 4 $FePO_4$/HA HHCF cycles. Conditions: $[SM2]_0$ = 5 mg/L, $[FePO_4]_0$ = 0.4 g/L, $[H_2O_2]_0$ = 5 mmol/L, $[HA]_0$ = 1 mmol/L, initial pH was not adjusted, ca. 4.3.

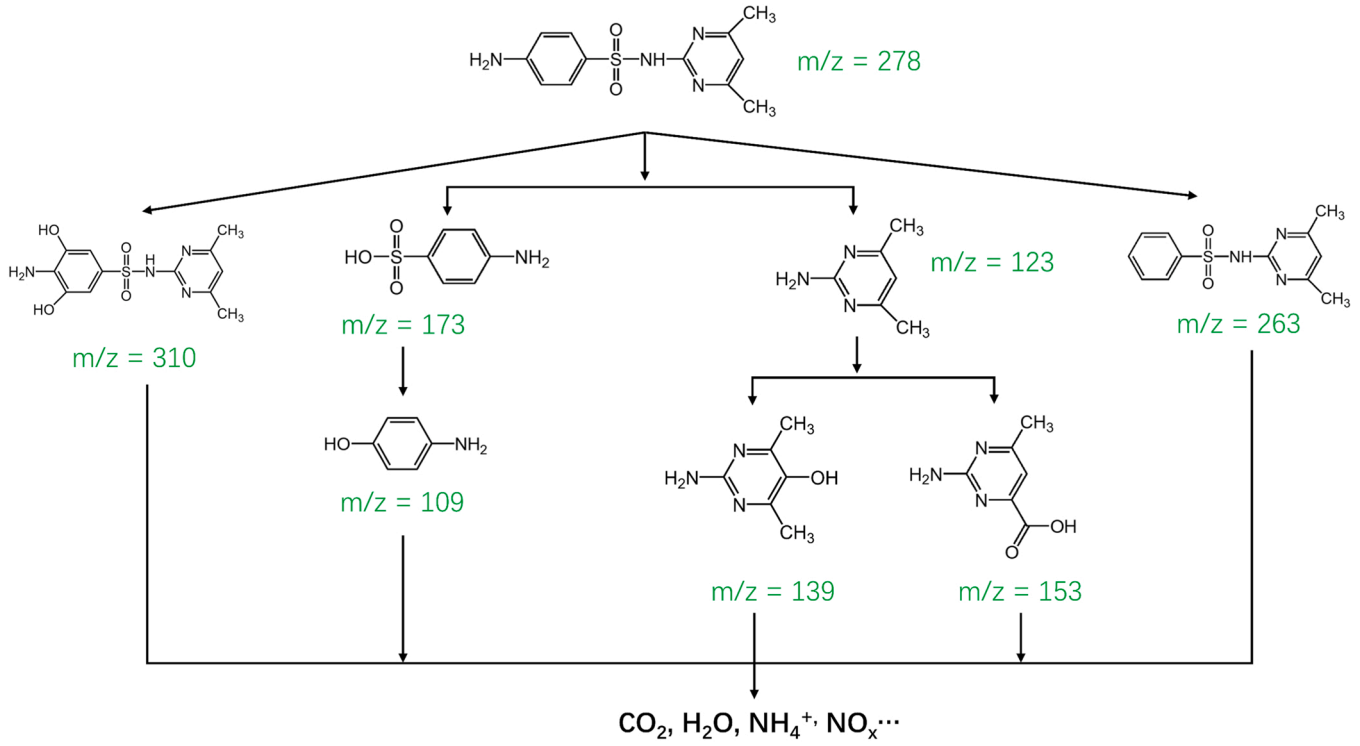

Scheme 1. The possible pathways of SM2 degradation during the $FePO_4$/HA HHCF process.

14.0 mg/L (1 mmol/L HA). After 100 min of reaction, 8.9 mg/L of HA-N was consumed, producing 4.3 mg/L NO_3^--N and 2.3 mg/L gaseous N, as calculated with the decrease of TN. NH_4^+-N and NO_2^--N were not detected (Fig. 7a). As for the $FePO_4$/HA HHCF system with SM2, the initial TN was also 12.8 mg/L although the theoretical N concentration slightly increased to 14.9 mg/L. After 100 min of reaction, 4.5 mg/L HA-N and 0.9 mg/L SM2-N were consumed, generating 0.3 mg/L NH_4^+-N, 0.4 mg/L NO_2^--N, 0.4 mg/L NO_3^--N, and 1.9 mg/L gaseous N (Fig. 7b). HA was mainly oxidized to nitrate by •OH in the absence of SM2, but changed to gaseous products such as N_2 in the presence of SM2, lowering the risk of nitrogen residual. Nitrogen in SM2 was possibly converted to ammonia, which would be further oxidized. Fortunately, the final concentrations of NH_4^+-N and TN were much below the Discharge Standards of NH_4^+-N (5 mg/L) and TN (15 mg/L) for Municipal Wastewater Treatment Plant (GB 18918-2002, China).

4. Conclusions

In this study, we have demonstrated that the combination of H_2O_2, ferric phosphate and hydroxylamine can offer a highly efficient heterogeneous-homogeneous coupled Fenton process for the oxidation of antibiotics sulfamethazine. In this new Fenton process,

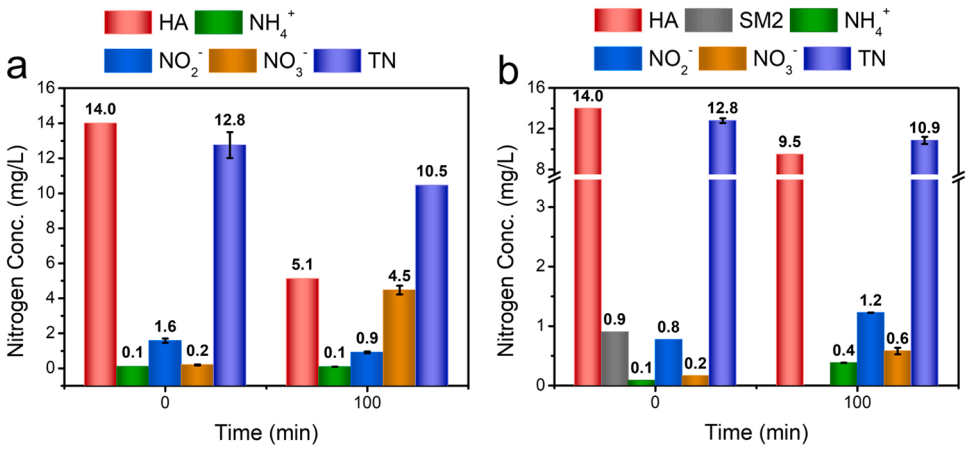

Fig. 7. The transformation of nitrogen during the $FePO_4$/HA HHCF treatment, (a) in the absence of SM2 and (b) in the presence of SM2. Conditions: $[SM2]_0 = 5$ mg/L, $[FePO_4]_0 = 0.4$ g/L, $[H_2O_2]_0 = 5$ mmol/L, $[HA]_0 = 1$ mmol/L, initial pH was not adjusted (4.3).

hydroxylamine could efficiently promote the desirable dissolution of iron from $FePO_4$, and also promote the subsequent redox cycle of Fe(III)/Fe(II) in the bulk solution to boost the conversion of H_2O_2 to •OH with a yield as high as 57.4%. Meanwhile, the competitive •OH consumption of hydroxylamine was much less than that of organic group contained iron cycle mediators such as ascorbic acid, leaving behind more •OH for the removal of sulfamethazine. Compared with other iron-bearing minerals including magnetite and hematite, $FePO_4$ was a superior heterogeneous-homogeneous coupled Fenton catalyst by means of its suitable iron dissolution ability and excellent reusability. More importantly, the phosphorus release from ferric phosphate and the nitrogen residual during this new Fenton process were limited to reduce the environmental risk of secondary pollution. This study highlights the importance of iron cycle and effective utilization of •OH on the Fenton degradation of organic pollutants, and provides a new strategy to develop highly efficient Fenton systems for pollutant control and environmental remediation.

CRediT authorship contribution statement

Hanjie Zhang: Investigation, Visualization, Validation. **Linghan Li:** Investigation. **Na Chen:** Conceptualization, Formal analysis. **Haijie Ben:** Validation. **Guangming Zhan:** Visualization, **Hongwei Sun:** Methodology, Writing - Original Draft, Funding acquisition. **Qin Li:** Writing - Review & Editing, Funding acquisition. **Jie Sun:** Supervision. **Lizhi Zhang:** Conceptualization, Supervision, Funding acquisition, Writing - Review & Editing.

Declaration of Competing Interest

The authors declare that they have no known competing financial interests or personal relationships that could have appeared to influence the work reported in this paper.

Acknowledgment

This work was financially supported by the National Key Research and Development Program of China (Grant 2018YFC1802003), the National Natural Science Foundation of China (Grant 22076061, 21936003), and National Innovation and Entrepreneurship Training Program for College Students, South-central University for Nationalities (Grant 202110524009).

Appendix A. Supporting information

Supplementary data associated with this article can be found in the online version at doi:10.1016/j.apcatb.2022.121410.

References

[1] J.J. Pignatello, E. Oliveros, A. MacKay, Advanced oxidation processes for organic contaminant destruction based on the Fenton reaction and related chemistry, Crit. Rev. Environ. Sci. Technol. 36 (2006) 1–84.
[2] E. Brillas, I. Sirés, M.A. Oturan, Electro-Fenton process and related electrochemical technologies based on Fenton's reaction chemistry, Chem. Rev. 109 (2009) 6570–6631.
[3] N. Wang, T. Zheng, G. Zhang, P. Wang, A review on Fenton-like processes for organic wastewater treatment, J. Environ. Chem. Eng. 4 (2016) 762–787.
[4] M. Zhang, H. Dong, L. Zhao, D. Wang, D. Meng, A review on Fenton process for organic wastewater treatment based on optimization perspective, Sci. Total Environ. 670 (2019) 110–121.
[5] Y. Zhu, R. Zhu, Y. Xi, J. Zhu, G. Zhu, H. He, Strategies for enhancing the heterogeneous Fenton catalytic reactivity: a review, Appl. Catal. B-Environ. 255 (2019), 117739.
[6] Y. Gao, W. Zhu, J. Liu, P. Lin, J. Zhang, T. Huang, K. Liu, Mesoporous sulfur-doped $CoFe_2O_4$ as a new Fenton catalyst for the highly efficient pollutants removal, Appl. Catal. B-Environ. 295 (2021), 120273.
[7] Y. Shi, X. Wang, X. Liu, C. Ling, W. Shen, L. Zhang, Visible light promoted Fe_3S_4 Fenton oxidation of atrazine, Appl. Catal. B-Environ. 277 (2020), 119229.
[8] M. Munoz, Z.M. de Pedro, J.A. Casas, J.J. Rodriguez, Preparation of magnetite-based catalysts and their application in heterogeneous Fenton oxidation - a review, Appl. Catal. B-Environ. 176–177 (2015) 249–265.
[9] X. Nie, G. Li, S. Li, Y. Luo, W. Luo, Q. Wan, T. An, Highly efficient adsorption and catalytic degradation of ciprofloxacin by a novel heterogeneous Fenton catalyst of hexapod-like pyrite nanosheets mineral clusters, Appl. Catal. B-Environ. 300 (2022), 120734.
[10] G.P. Anipsitakis, D.D. Dionysiou, Radical Generation by the interaction of transition metals with common oxidants, Environ. Sci. Technol. 38 (2004) 3705–3712.
[11] E.G. Garrido-Ramírez, B.K.G. Theng, M.L. Mora, Clays and oxide minerals as catalysts and nanocatalysts in Fenton-like reactions - a review, Appl. Clay Sci. 47 (2010) 182–192.
[12] S.O. Ganiyu, M. Zhou, C.A. Martinez-Huitle, Heterogeneous electro-Fenton and photoelectro-Fenton processes: a critical review of fundamental principles and application for water/wastewater treatment, Appl. Catal. B-Environ. 235 (2018) 103–129.
[13] S. Rahim Pouran, A.A. Abdul Raman, W.M.A. Wan Daud, Review on the application of modified iron oxides as heterogeneous catalysts in Fenton reactions, J. Clean. Prod. 64 (2014) 24–35.
[14] J. He, X. Yang, B. Men, D. Wang, Interfacial mechanisms of heterogeneous Fenton reactions catalyzed by iron-based materials: a review, J. Environ. Sci. 39 (2016) 97–109.
[15] A.V. Vorontsov, Advancing Fenton and photo-Fenton water treatment through the catalyst design, J. Hazard. Mater. 372 (2019) 103–112.
[16] M.M. Bello, A.A. Abdul Raman, A. Asghar, A review on approaches for addressing the limitations of Fenton oxidation for recalcitrant wastewater treatment, Process Saf. Environ. 126 (2019) 119–140.
[17] J.F. Barona, D.F. Morales, L.F. González-Bahamón, C. Pulgarín, L.N. Benítez, Shift from heterogeneous to homogeneous catalysis during resorcinol degradation using the solar photo-Fenton process initiated at circumneutral pH, Appl. Catal. B-Environ. 165 (2015) 620–627.
[18] J. He, X. Yang, B. Men, L. Yu, D. Wang, EDTA enhanced heterogeneous Fenton oxidation of dimethyl phthalate catalyzed by Fe_3O_4: Kinetics and interface mechanism, J. Mol. Catal. A-Chem. 408 (2015) 179–188.

[19] L. Xu, J. Wang, Fenton-like degradation of 2,4-dichlorophenol using Fe_3O_4 magnetic nanoparticles, Appl. Catal. B-Environ. 123–124 (2012) 117–126.
[20] X. Xue, K. Hanna, C. Despas, F. Wu, N. Deng, Effect of chelating agent on the oxidation rate of PCP in the magnetite/H_2O_2 system at neutral pH, J. Mol. Catal. A-Chem. 311 (2009) 29–35.
[21] T. Xu, Y. Fang, T. Tong, Y. Xia, X. Liu, L. Zhang, Environmental photochemistry in hematite-oxalate system: Fe(III)-Oxalate complex photolysis and ROS generation, Appl. Catal. B-Environ. 283 (2021), 119645.
[22] Y. Baba, T. Yatagai, T. Harada, Y. Kawase, Hydroxyl radical generation in the photo-Fenton process: effects of carboxylic acids on iron redox cycling, Chem. Eng. J. 277 (2015) 229–241.
[23] H. Sun, G. Xie, D. He, L. Zhang, Ascorbic acid promoted magnetite Fenton degradation of alachlor: mechanistic insights and kinetic modeling, Appl. Catal. B-Environ. 267 (2020), 118383.
[24] S. Zhou, Y. Yu, J. Sun, S. Zhu, J. Deng, Oxidation of microcystin-LR by copper (II) coupled with ascorbic acid: kinetic modeling towards generation of H_2O_2, Chem. Eng. J. 333 (2018) 443–450.
[25] S. Zhou, Y. Yu, W. Zhang, X. Meng, J. Luo, L. Deng, Z. Shi, J. Crittenden, Oxidation of microcystin-LR via activation of peroxymonosulfate using ascorbic acid: kinetic modeling and toxicity assessment, Environ. Sci. Technol. 52 (2018) 4305–4312.
[26] Z. Li, L. Wang, Y. Liu, Q. Zhao, J. Ma, Unraveling the interaction of hydroxylamine and Fe(III) in Fe(II)/Persulfate system: a kinetic and simulating study, Water Res. 168 (2020), 115093.
[27] X. Wang, N. Chen, X. Liu, Y. Shi, C. Ling, L. Zhang, Ascorbate guided conversion of hydrogen peroxide to hydroxyl radical on goethite, Appl. Catal. B-Environ. 282 (2021), 119558.
[28] X. Hou, X. Huang, F. Jia, Z. Ai, J. Zhao, L. Zhang, Hydroxylamine promoted goethite surface Fenton degradation of organic pollutants, Environ. Sci. Technol. 51 (2017) 5118–5126.
[29] L. Chen, X. Li, J. Zhang, J. Fang, Y. Huang, P. Wang, J. Ma, Production of hydroxyl radical via the activation of hydrogen peroxide by hydroxylamine, Environ. Sci. Technol. 49 (2015) 10373–10379.
[30] X. Liu, C. He, Z. Shen, W. Li, N. Chen, J. Song, X. Zhou, Y. Mu, Mechanistic study of Fe(III) chelate reduction in a neutral electro-Fenton process, Appl. Catal. B-Environ. 278 (2020), 119347.
[31] L. Wei, Y. Zhang, S. Chen, L. Zhu, X. Liu, L. Kong, L. Wang, Synthesis of nitrogen-doped carbon nanotubes-$FePO_4$ composite from phosphate residue and its application as effective Fenton-like catalyst for dye degradation, J. Environ. Sci. 76 (2019) 188–198.
[32] N. Chen, Y. Huang, X. Hou, Z. Ai, L. Zhang, Photochemistry of hydrochar: reactive oxygen species generation and sulfadimidine degradation, Environ. Sci. Technol. 51 (2017) 11278–11287.
[33] N. Chen, H. Shang, S. Tao, X. Wang, G. Zhan, H. Li, Z. Ai, J. Yang, L. Zhang, Visible light driven organic pollutants degradation with hydrothermally carbonized sewage sludge and oxalate via molecular oxygen activation, Environ. Sci. Technol. 52 (2018) 12656–12666.
[34] H. Sun, F. He, W. Choi, Production of reactive oxygen species by the reaction of periodate and hydroxylamine for rapid removal of organic pollutants and waterborne bacteria, Environ. Sci. Technol. 54 (2020) 6427–6437.
[35] G.W. Klein, K. Bhatla, V. Madhavan, R.H. Schuler, Reaction of hydroxyl radicals with benzoic acid. Isomer distribution in the radical intermediates, J. Phys. Chem. 79 (1975) 1767–1774.
[36] M.E. Lindsey, M.A. Tarr, Quantitation of hydroxyl radical during Fenton oxidation following a single addition of iron and peroxide, Chemosphere 41 (2000) 409–417.
[37] A.E. Harvey, J.A. Smart, E.S. Amis, Simultaneous spectrophotometric determination of iron(II) and total iron with 1,10-phenanthroline, Anal. Chem. 27 (1955) 26–29.
[38] S.P. Schwaminger, D. Bauer, P. Fraga-García, F.E. Wagner, S. Berensmeier, Oxidation of magnetite nanoparticles: Impact on surface and crystal properties, CrystEngComm 19 (2017) 246–255.
[39] J. Duan, S. Pang, Z. Wang, Y. Zhou, Y. Gao, J. Li, Q. Guo, J. Jiang, Hydroxylamine driven advanced oxidation processes for water treatment: a review, Chemosphere 262 (2021), 128390.
[40] L. Chen, J. Ma, X. Li, J. Zhang, J. Fang, Y. Guan, P. Xie, Strong enhancement on Fenton oxidation by addition of hydroxylamine to accelerate the ferric and ferrous iron cycles, Environ. Sci. Technol. 45 (2011) 3925–3930.
[41] X. Wu, X. Gu, S. Lu, Z. Qiu, Q. Sui, X. Zang, Z. Miao, M. Xu, Strong enhancement of trichloroethylene degradation in ferrous ion activated persulfate system by promoting ferric and ferrous ion cycles with hydroxylamine, Sep. Purif. Technol. 147 (2015) 186–193.
[42] S. Fukuchi, R. Nishimoto, M. Fukushima, Q. Zhu, Effects of reducing agents on the degradation of 2,4,6-tribromophenol in a heterogeneous Fenton-like system with an iron-loaded natural zeolite, Appl. Catal. B-Environ. 147 (2014) 411–419.
[43] Y. Feng, D. Wu, Y. Zhou, K. Shih, A metal-free method of generating sulfate radicals through direct interaction of hydroxylamine and peroxymonosulfate: mechanisms, kinetics, and implications, Chem. Eng. J. 330 (2017) 906–913.
[44] J. Yang, J. Li, W. Dong, J. Ma, J. Cao, T. Li, J. Li, J. Gu, P. Liu, Study on enhanced degradation of atrazine by ozonation in the presence of hydroxylamine, J. Hazard Mater. 316 (2016) 110–121.
[45] J. Lu, Y. Lei, J. Ma, X. Liu, M. Zhu, C. Zhu, Photochemical reaction kinetics and mechanistic investigations of nitrous acid with sulfamethazine in tropospheric water, Environ. Sci. Pollut. Res. Int. 26 (2019) 26134–26145.
[46] H. Li, J. Shang, Z. Yang, W. Shen, Z. Ai, L. Zhang, Oxygen vacancy associated surface Fenton chemistry: surface structure dependent hydroxyl radicals generation and substrate dependent reactivity, Environ. Sci. Technol. 51 (2017) 5685–5694.
[47] Y. Liu, J. Wang, Degradation of sulfamethazine by gamma irradiation in the presence of hydrogen peroxide, J. Hazard. Mater. 250–251 (2013) 99–105.
[48] B. Yang, X. Mao, L. Pi, Y. Wu, H. Ding, W. Zhang, Effect of pH on the adsorption and photocatalytic degradation of sulfadimidine in Vis/g-C_3N_4 progress, Environ. Sci. Pollut. Res. Int. 24 (2017) 8658–8670.
[49] C. Zhou, C. Lai, P. Xu, G. Zeng, D. Huang, C. Zhang, M. Cheng, L. Hu, J. Wan, Y. Liu, W. Xiong, Y. Deng, M. Wen, In situ grown AgI/$Bi_{12}O_{17}Cl_2$ heterojunction photocatalysts for visible light degradation of sulfamethazine: efficiency, pathway, and mechanism, ACS Sustain. Chem. Eng. 6 (2018) 4174–4184.
[50] S. Fukahori, T. Fujiwara, Photocatalytic decomposition behavior and reaction pathway of sulfamethazine antibiotic using TiO_2, J. Environ. Manag. 157 (2015) 103–110.